Colloids and Surfaces A 541 (2018) 97–107

Contents lists available at ScienceDirect

Colloids and Surfaces A

journal homepage: www.elsevier.com/locate/colsurfa

Sequential synthesis of a magnetic nano-adsorbent: How the first step identifies the final product

Mehdi Safdarian[a], Zahra Ramezani[a,b,*]

[a] Nanotechnology Research Centre, Ahvaz Jundishapur University of Medical Sciences, Ahvaz, Iran
[b] Medicinal Chemistry Department, Faculty of Pharmacy, Ahvaz Jundishapur University of Medical Sciences, Ahvaz, Iran

GRAPHICAL ABSTRACT

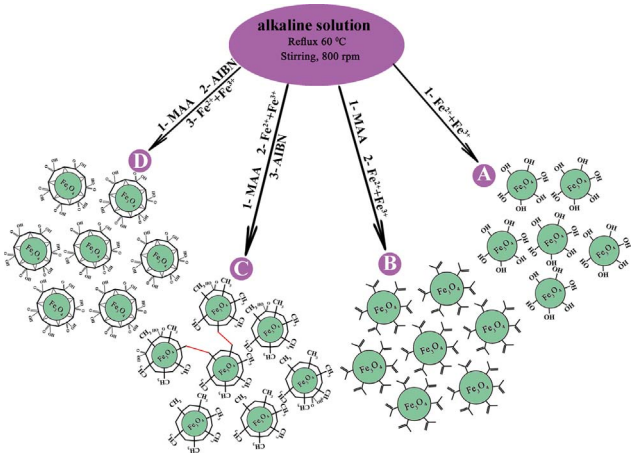

ARTICLE INFO

Keywords:
Hydrophobic magnetite
Hydrophilic magnetite
Modified magnetite
Magnetic polymers
Nanoparticles dispersion

ABSTRACT

Three types of super paramagnetic core-shell nanoparticles have creatively been synthesized via three basic substances, Fe^{2+}/Fe^{3+}, methacrylic acid (MAA), and 2,2′-azobisisobutyronitrile (AIBN). It has been demonstrated that the order of addition of starting materials determines the type of products. Methacrylic acid coated magnetic nanoparticles (Fe_3O_4@MAA) with abundant double bonds on the surface, poly methacrylic acid coated magnetic nano particles (Fe_3O_4@PMAA) having plenty of surface carboxylic groups, and amphiphilic shell of methacrylic acid polymer on magnetic nano particles core (Fe_3O_4@AMPH) having both carboxyl and alkyl groups on the surface were prepared in three, separate one-pot, sequential synthesis. At first, the resultant magnetic nanoparticles (MNPs) were characterized by transmission electron microscopy (TEM), dynamic light scattering, X-ray spectroscopy, Fourier transform infrared spectroscopy (FTIR) and thermal analysis. Then, the colloidal stability of the synthesized particles was investigated in several common solvents such as water, 1-propanol, chloroform, and edible oil. Finally, the application of each nanoparticle was discussed. It was found that Fe_3O_4@MAA can be successfully applied as a core in polymerization procedure. Fe_3O_4@PMAA performed well in nickel uptake and can therefore be used as magnetic solid sorbent in nickel pre-concentration and re-

* Corresponding author at: Nanotechnology Research Centre, Ahvaz Jundishapur University of Medical Sciences, Ahvaz, Iran.
E-mail address: zramezani@ajums.ac.ir (Z. Ramezani).

https://doi.org/10.1016/j.colsurfa.2018.01.004
Received 13 October 2017; Received in revised form 30 December 2017; Accepted 2 January 2018
Available online 12 January 2018
0927-7757/

mediation. Fe_3O_4@AMPH was well dispersed in oil, suggesting that it can be successfully used as a good extractor in dispersive solid phase pre-concentration and cleanup of both hydrophilic and hydrophobic compounds in heated edible oil samples.

1. Introduction

Magnetic nanoparticles (MNPs) have shown considerable promise for a vast variety of applications. In most cases, modification of the magnetic material and colloidal stability of their suspensions are of vital importance. Controlling the surface chemistry of MNPs through surface modification is required not only to prevent the aggregation of MNPs, leading to colloidal stability [1], but also to render them with water and organic solvent dispersibility [2,3], and biocompatibility [4,5]. Their chemical stability and targeting can be increased as well [6,7]. Control of the surface chemistry of MNPs provides the particles with specific characterization and extends their fields of application. Therefore, functionalized MNPs have attracted many attentions for a wide variety of applications such as metal pre-concentration [8,9], magnetic resonance imaging (MRI) [10], being used as catalysts [11,12], surface polymerization [13,14], drug delivery [15,16] and so forth.

Fe_3O_4 nanoparticles, as the most widely-used member of MNPs, has super-paramagnetic properties as well as a good physical and chemical stability making it suitable as a core in preparation of magnetic sorbents in magnetic solid-phase extractions (MSPE) [17–19]. Hydrophobic Fe_3O_4 magnetic nanoparticles had been prepared in two steps namely, Fe_3O_4 nanoparticles synthesis and then its modification [3,20]. Synthesis of polymer coated Fe_3O_4 has been reported in two or three steps. In the reported procedures, the first step was preparation of Fe_3O_4 nanoparticles, in the second step the particles were modified with silicon based compound such as 3-methacryloxy propyl trimethoxy silane or oleic acid [20–25] in order to provide abundant double bond to start polymerization, and finally polymerization happened. The disadvantage of these protocols are, the overall time of the reaction is high, they take more operator time, and it is not economic due to consumption of different reagents. Recently, the one-pot synthesis of coated MNPs has attracted the attention of many scientists [26–29]. A simple and fast protocol for preparing MNPs is still a big challenge. In one-pot synthesis methodology, order of addition of the reagents is very important and determines the target nanoparticles (NPs) through controlling the proper functional group on the surface [30]. In recent one pot synthesis of Fe_3O_4@PMAA, methacrylic acid polymer was used as starting material [31,32].

magnetic particles are extensively used in separation, cleanup and pre-concentration of environmental [20], food [22], and clinical [33] samples prior to instrumental analysis, mainly because of ease in separation of particles by an external magnet. Polymer coated Fe_3O_4 having plenty of carboxylic groups on the surface could be a good adsorbent for metal ions through complex formation. Amphiphilic MNPs can easily be dispersed in hydrophilic and hydrophobic media, and consequently used for separation of polar or non-polar analyte. Therefore, facile modification procedure of the particles as well as dispersibility in the target media is of interest, in particles preparation for the specific applications.

This study reports three parallel one-pot experiments each having the same starting materials but differing in their order of addition in an alkali solution. Three different coated Fe_3O_4 MNPs with different colloidal stabilities and polarities were produced. After characterizing each of the MNPs, an application for each synthesized particle was introduced. Dispersion of the particles in different solvents was also evaluated. It was concluded that long time dispersion of the particles in the solvents depends on their surface functional groups. With the introduction of simple synthetic methodology, stable colloid magnetic nanomaterial that can efficiently be used in environmental, biomedical and analytical researches is produced.

2. Experimental

2.1. Reagents and materials

The chemicals used in the experiments including Iron (III) chloride hexahydrate ($FeCl_3{\cdot}6H_2O$), iron (II) chloride tetrahydrate ($FeCl_2{\cdot}4H_2O$), methanol (MeOH), ethanol (EtOH), 1-propanol (1-PPOH), 1-butanol (1-BuOH), chloroform, hydrochloric acid, glacial acetic acid (HOAC) as well as some other chemicals were purchased from Merck (Darmstadt, Germany) and were used without additional purification. Methacrylic acid (MAA) and 2, 2′-azobisisobutyronitrile (AIBN) were bought from Sigma–Aldrich (St. Louis, MO). Deionized water (DI water) was used whenever required. Edible oil was purchased from local markets in Ahvaz, Khozestan, Iran.

2.2. Synthesis of nanoparticles

Fig. 1 schematically shows conditions for synthesis of magnetite and its three different modified forms in three separate one-pot experiments. Details of each protocol are explained in the following sections.

2.2.1. Fe_3O_4 nanoparticles

The magnetite nanoparticles (Fe_3O_4) were prepared via the conventional co-precipitation method with slight modifications [34]. $FeCl_3{\cdot}6H_2O$ (10 mmol) and $FeCl_2{\cdot}4H_2O$ (5 mmol) were dissolved in 1 mol L^{-1} HCl (50 mL). Then, Fe_3O_4 magnetic nanoparticles were produced by drop-wise addition of the resulting solution to an alkaline solution (100 mL, NaOH 2 M) under nitrogen atmosphere at reflux conditions at 60 °C while being stirred magnetically at 800 rpm (Fig. 1A). Stirring was continued for 1 h. Finally, the obtained black precipitates were separated by an external permanent magnet (1.4 T) and washed repeatedly with deionized water until filtrate became neutral, and then lyophilized.

2.2.2. Fe_3O_4@MAA nanoparticles

In the second experiment, the alkaline solution in Section 2.2.1 was replaced by alkaline MAA solution. The experiments were followed as explained in Section 2.2.1. Briefly, 2 mL MAA was added to 10 mL 2 mol L^{-1} NaOH. Then 50 mL Fe^{3+}/Fe^{2+} solution was added to the alkaline MMA solution under N_2 atmosphere while being refluxed at 60 °C and stirred at 800 rpm (Fig. 1B). The black precipitates of Fe_3O_4@MAA were magnetically collected and washed repeatedly with deionized water until the pH of the filtrate became neutral. Then, it was lyophilized and put aside for future use.

2.2.3. Fe_3O_4@AMPH nanoparticles

In the third experiment, the same protocols as described in Section 2.2.2 were performed for one-pot synthesis of Fe_3O_4@AMPH. However, before collecting Fe_3O_4@MAA nanoparticles, 1 mmol of AIBN was added to the mixture and stirred for 1 h. Consequently, MAA polymerization occurred on the surface. Finally, the resultant nanoparticles were magnetically collected and washed repeatedly with deionized water and lyophilized for further use (Fig. 1C).

2.2.4. Fe_3O_4@PMAA nanoparticles

A mixture of 2 mL MAA and 1 mmol AIBN in 2 mol L^{-1} NaOH (100 mL) were prepared and magnetically stirred with 800 rpm for 15 min while refluxing at 60 °C. Then Fe^{3+}/Fe^{2+} solution (50 mL) was

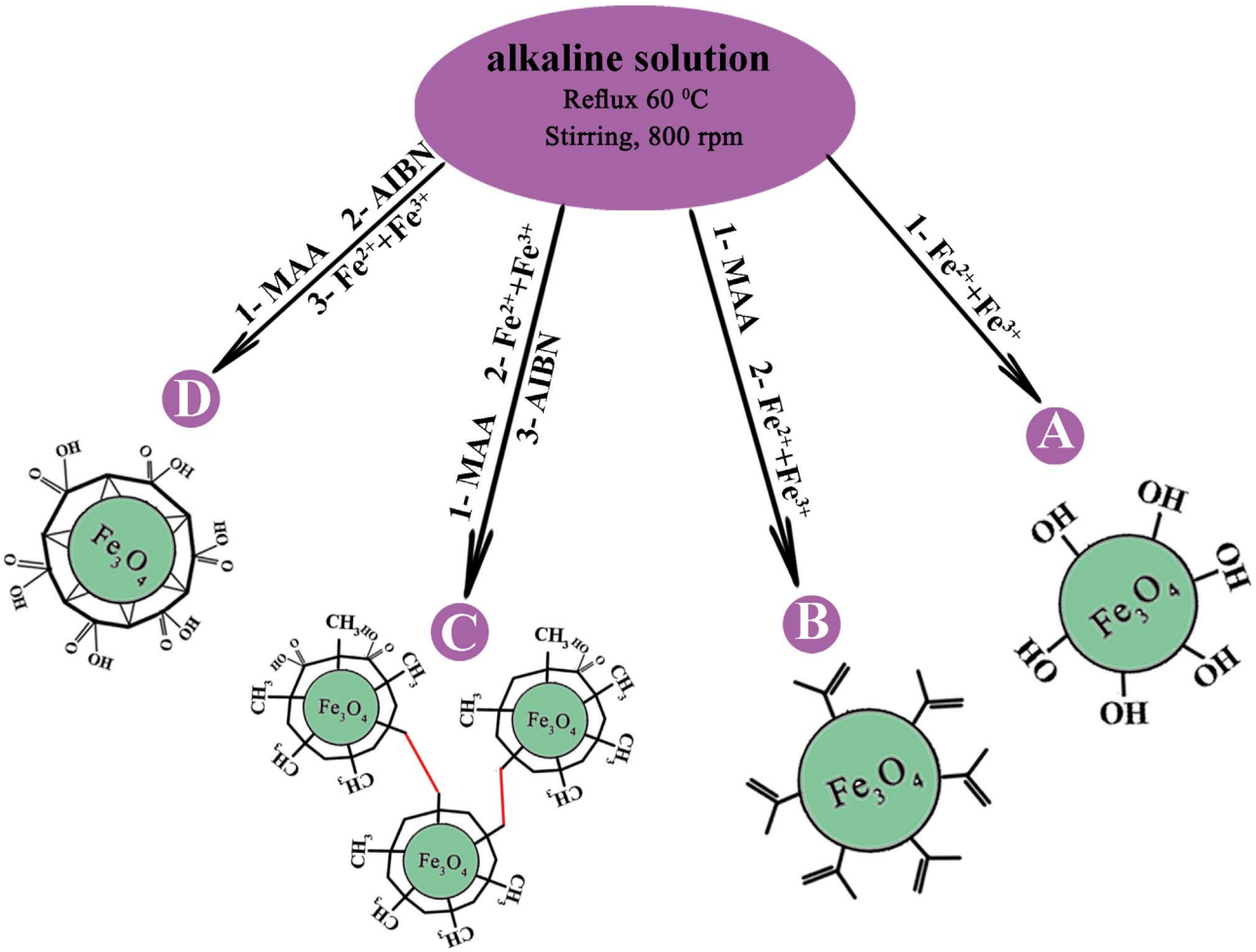

Fig. 1. Schematic representation of the trends in sequential synthesis of magnetic nanoparticles. Preparation path for A) nano Fe_3O_4, B) Fe_3O_4@MAA, C) Fe_3O_4@AMPH, D) Fe_3O_4@PMAA.

added to the mixture under N_2 atmosphere. Finally, the resultant nanoparticles, named Fe_3O_4@PMAA, were magnetically collected and washed repeatedly with deionized water and lyophilized (Fig. 1D).

2.3. Characterization

Core shell properties and the particle size of the materials were observed by an EM 10 C-80 KV transmission electron microscope (Zeiss, Germany) operating at an acceleration voltage of 80 kV. As-prepared MNPs were dispersed in DI water and coated onto carbon coated copper grid, dried and put under TEM microscope for morphology and size evaluations. XRD patterns for four synthetized particles was reordered by PW-1840 Philips diffractometer with Cu K_α radiation wavelength of 1.5418°A. Particle size analysis (PSA) of as prepared particles was determined by dynamic light scattering (Scatteroscope I, Qudix, Korea). Thermo gravimetric analysis (TGA) was performed on a STA503 instrument (BÄHR-Thermo-analyse GmbH, Germany) from room temperature to 600 °C with a heating rate of 10 °C min^{-1} in a nitrogen flow (100 mL min^{-1}). Fourier transform infrared (FTIR) spectra were recorded on a vertex 70 FTIR spectrometer (Bruker, Germany). The magnetic properties were measured using MDK-VSM system (Meghnatis Daghigh Daneshpajouh Co., Iran).

2.4. Nanoparticles dispersion study

Dispersion of the prepared Fe_3O_4@AMPH and Fe_3O_4@PMAA particles was studied at concentration of 1 mg ml^{-1} in different solvents such as water, 1-propanol, chloroform and edible oil. Dispersivity of the Fe_3O_4@ AMPH particles were evaluated in different volume percent of EtOH. The photographs of the resultant suspension were captured at different time intervals just from the start of experiment by an 18.2 megapixel resolution digital camera (Sony Cyber-shot, DSC-WX300).

2.5. Ni^{2+} adsorption by Fe_3O_4@PMAA

To evaluate Ni^{2+} adsorption ability of Fe_3O_4@PMAA, a certain amount of Fe_3O_4@PMAA suspension was mixed with 10 mL of 10 mg L^{-1} Ni^{2+} solution at pH 8 adjusted by ammonium buffer for 1 min. The particles were then magnetically separated and washed with double ionized water for several times and dried. FTIR spectrum of dried nickel loaded Fe_3O_4@PMAA was recorded.

An AAS-vario6 Analytik Jena graphite furnace atomic absorption spectrometer (GFAAS) was sued for the determination of nickel concentration.

For adsorption kinetic studies, 50 mL of 0.5 ppm Ni^{2+} solution got into contact with Fe_3O_4@PMAA at pH 8 (in ammonium buffer) for different times. Equilibrium concentration was determined after the filtration of the solution at different time intervals by GFAAS.

2.6. Edible oil volatile compound GC/MS

2.6.1. GC/MS conditions

Gas chromatography mass spectrometric analysis (GC/MS) was performed using a 7890A Agilent gas chromatograph (Agilent, Little

Falls, DE, USA) equipped with a MSD-5975C mass selective detector and a CTC CombiPAL auto sampler (Zwingen, Switzerland). Instrument control and data collection was provided by Chemstation software version 5.51. Wiley 7.1 and NIST 5.0a spectral libraries were used to identify the compounds. CombiPAL was set for head space sampling. The PAL program was as follows: head space syringe temperature 60 °C, incubation temperature and time for vial containing sample were 100 °C and 10 min, respectively while agitated at 500 rpm. Consequently, the injection speed and volume were 500 μL S^{-1} and 50 μL. A HP-5MS (30 m × 0.320 mm; 0.25 μm) was used for volatile organic compounds (VOCs) separations. Injection, auxiliary, and detector temperatures were set at 250 °C, 230 °C, and 150 °C, respectively.

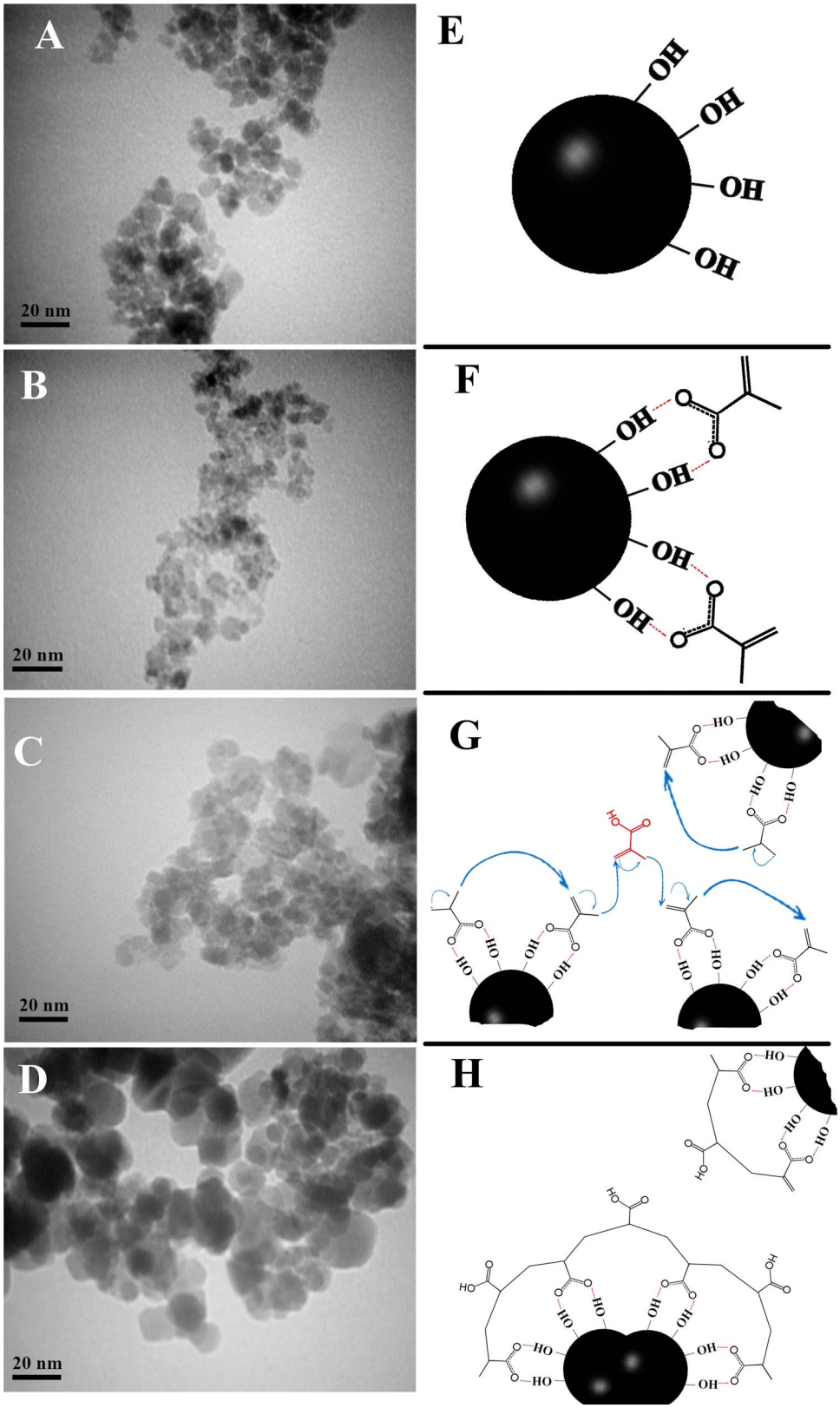

Fig. 2. TEM images of A: Fe_3O_4, B: Fe_3O_4@MAA, C: Fe_3O_4@AMPH and D: Fe_3O_4@PMAA nanoparticles. E through G show structural representation and possible mechanism for particle formation.

Carrier gas was high purity helium with a flow rate of 1 mL min^{-1}. Oven temperature was set at 35 °C and held at this temperature for 5 min. Then it was raised to 100 °C with 4 °C min^{-1}, stayed for 1 min and rose to 180 °C with 10 °C min^{-1}. It finally reached 250 °C with the rate of 15 °C min^{-1}. The total run time was estimated to be 35 min.

2.6.2. Sample preparations

Heated edible oil from fast food courts in Ahvaz, Iran was used for evaluating volatile organic contents (VOCs). VOCs' patterns were obtained by both static head space and solvent free magnetic dispersive solid phase extraction (recently introduce by our research group and will submit as soon as possible) with Fe_3O_4@AMPH as an amphiphilic sorbent. In static head space analysis of the oil volatiles, 0.5 and 10 mL of heated edible oil were individually placed in 20 mL Agilent head space vials and automatic head space sampling by the PAL system described in Section 2.6.1. In another experiments, 10 mL of heated edible oil was mixed with 5 mg Fe_3O_4@AMPH and stirred magnetically (500rpm) at 40 °C for 1 h in a closed 20 mL head space vial. Then, Fe_3O_4@AMPH was separated by a 1.4 T magnet. The vial containing solid Fe_3O_4@AMPH was placed in the GC auto sampler tray and analyzed as described in Section 2.6.1.

3. Results and discussion

As it is indicated in Fig. 1, the order of adding starting materials has a great influence on the specific features of the final modified magnetite. Each product was characterized by XRD, TEM, PSA, TGA, VSM and FTIR. Finally, dispersion of two polymer coated magnetite in different media and their possible analytical applications were discussed.

3.1. Characterization of nanoparticles

XRD analysis of Fe_3O_4, Fe_3O_4@MAA, Fe_3O_4@PMAA, and Fe_3O_4@AMPH are illustrated in Fig. S1 (see electronic Supplementary

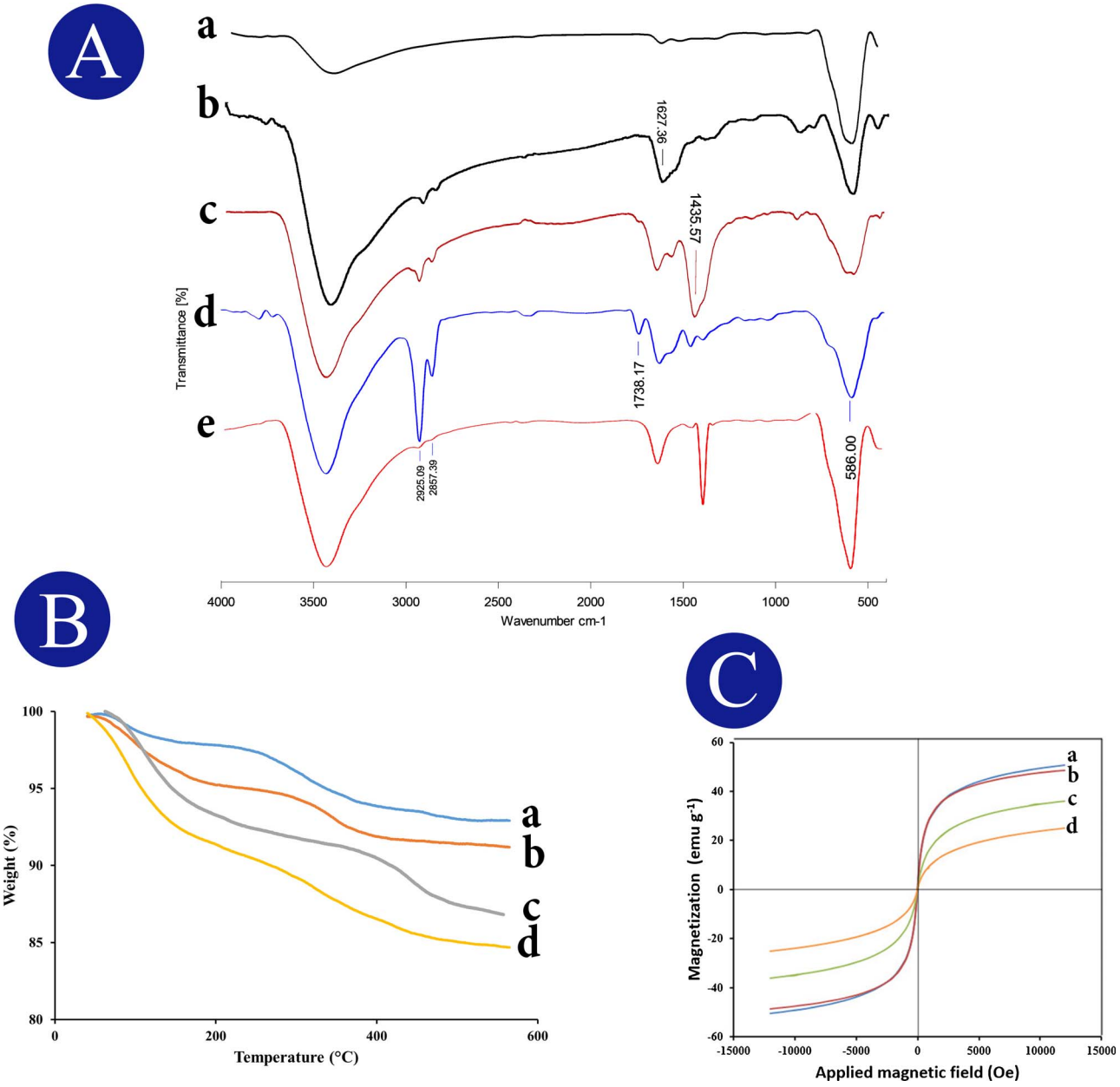

Fig. 3. A) FT-IR spectra of (a) bare Fe_3O_4 nanoparticles, (b) MAA functionalized Fe_3O_4 nanoparticles, (c) Fe_3O_4@AMPH (d) Fe_3O_4@PMAA (e) Fe_3O_4@PMAA nickel complex; B) TGA analysis of (a) Fe_3O_4, (b) Fe_3O_4@MAA, (c) Fe_3O_4@AMPH and (d) Fe_3O_4@PMAA; C) The hysteresis loop of (a) Fe_3O_4, (b) Fe_3O_4@MAA and (c) Fe_3O_4@AMPH and (d) Fe_3O_4@PMAA.

file). Characteristic peaks at 2θ = 30.06°, 35.44°, 43.09°, 53.57°, 56.93°, and 62.58° corresponding to (220), (311), (400), (422), (511), and (440) planes of Fe_3O_4, respectively[20] is observed in all synthesized particles.

Fig. 2 shows TEM images of the four synthesized MNPs. TEM images confirm that the Fe_3O_4 nanoparticles (Fig. 2A) are less poly-disperse than the others and have the mean diameter of 8 nm. A reduction in the size of Fe_3O_4@MAA compared to bare Fe_3O_4 is almost obvious in Fig. 2B. This may be due to the formation of a single layer of MAA shell on the surface of bare MNPs (Fig. 2F) that stabilize the particles and prevent their aggregation. From the image, the mean diameter of Fe_3O_4@MAA MNPs is estimated to be 5 nm. These data are consistence with hydrodynamic particle size reported in Table S1 and Fig. S2 and Fig. S3.

Fig. 2C indicates an increase in the size of MNPs after MAA polymerization on the surface of magnetite. The increase in size, was further confirmed by particle size analysis (using dynamic light scattering) reported in Table S1. This phenomenon can be further explained by the probable mechanism of MAA polymerization on the surface while adding AIBN to the synthesized Fe_3O_4@MAA. As it is shown in Fig. 2G, double bonds on the surface of two adjacent Fe_3O_4@MAA MNPs participate in polymerization reaction and connect the two particles. As a result, an increase in the final particle size is observed (Fig. 2G). It seems that a few MNPs connected together and a nanoparticle with mean diameter of 22.8 nm is produced (Table S1, electronic Supplementary file). Another possible mechanism is the interaction of two neighboring MAAs on the surface of a certain NP that produces a new polymeric particles without considerable increase in the final size

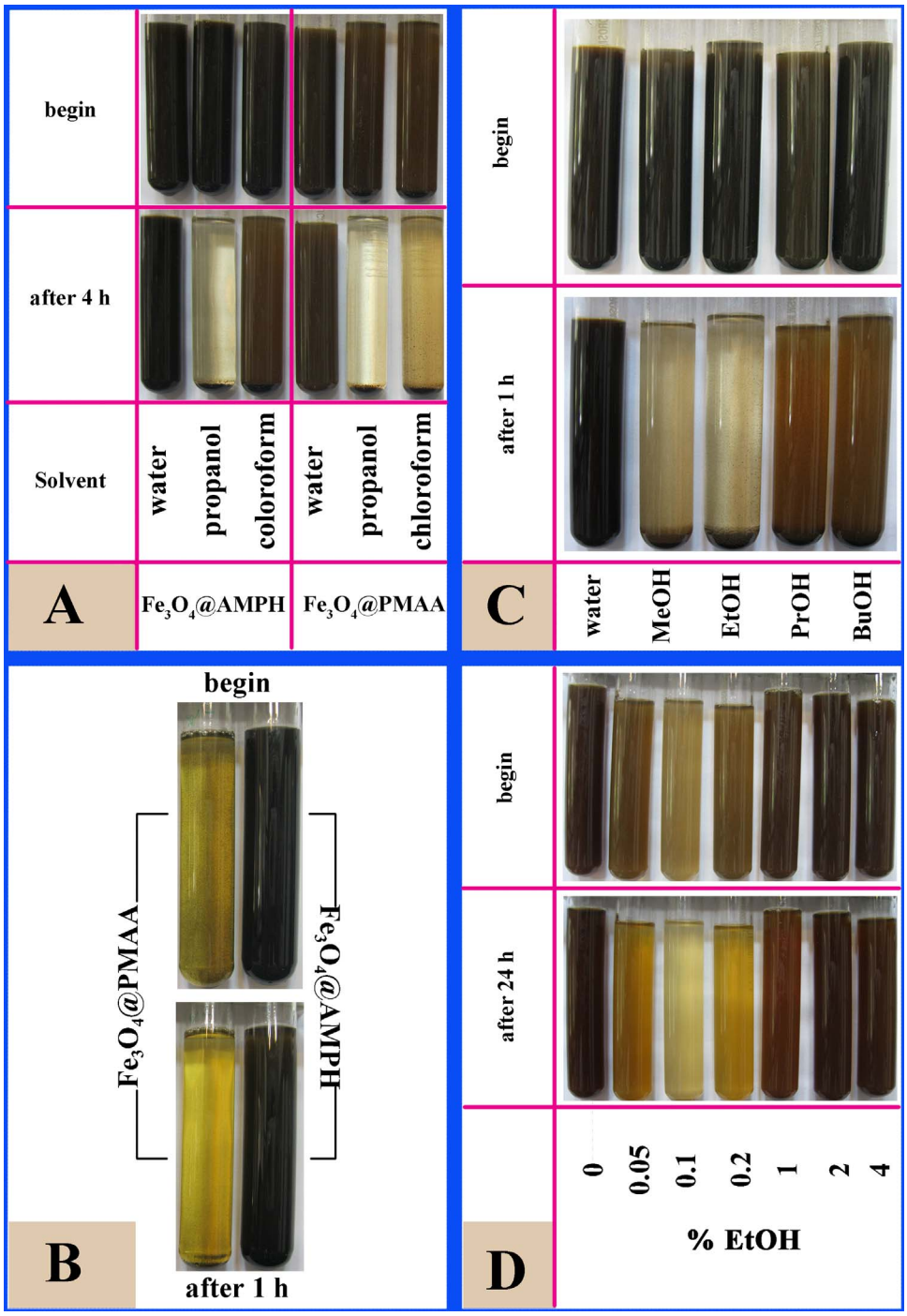

Fig. 4. Photographs showing solution stability of 1 mg ml^{-1} Fe_3O_4@AMPH and Fe_3O_4@PMAA in A: water, 1-propanol, and chloroform and B: edible oil; and Fe_3O_4@AMPH in C: more common alcohols and D: 0–4 v/v % EtOH.

(about 5.9–12.3 nm, see Table S1 in electronic Supplementary file) [35]. Therefore, big and small nanoclusters can be seen in Fig. 2C regarding different path for the formation of Fe_3O_4@AMPH MNPs. In Procedure 2.2.4., MAA polymerization starts before magnetite formation. Then PMAAs are attached to the surface of Fe_3O_4 with the probable mechanism that is shown in Fig. 2H. As a result, Fe_3O_4@PMAA with polar surface carboxylic groups (Fig. 2H), identified by FTIR data, is obtained and the produced particles have larger sizes relative to other coated MNPs. The size has been assumed larger, because of larger dark points in Fig. 2D compare to Fig. 2C and data in Table S1(electronic Supplementary file).To further characterize the particles and determine their functional groups, and evaluate the probable mechanism of formation FTIR spectra of bare Fe_3O_4, Fe_3O_4@MAA, Fe_3O_4@AMPH and Fe_3O_4@PMAA using KBr pellet were recorded as shown in Fig. 3. Modification in the particles was confirmed by both FTIR and TGA. The peak at 590 cm^{-1} in Fig. 3A (a) can be attributed to Fe–O band and the peak at 3388 cm^{-1} is the characteristic band of OH group, suggesting the formation of Fe_3O_4 MNPs. As is clear in Fig. 3B (b), the peak location of Fe–O is shifted from 590 cm^{-1} to 588 cm^{-1} [20]. A decrease in its intensity compare to carboxylic group in FTIR spectrum of Fe_3O_4@MAA MNPs is also noticed. Moreover, the OH band is shifted from 3388 Cm^{-1} in Fe_3O_4 to 3427 Cm^{-1} in Fe_3O_4@MAA and the peaks at 2926 cm^{-1} and 2858 cm^{-1} are originated from the asymmetric and symmetric stretching of CH_2. Vinyl groups peaking around 1627 cm^{-1} also appeared. These observations confirmed that the modification of Fe_3O_4 with MAA occurs through hydrogen bonding interaction [20]. Fig. 3B(a) and (b) exhibit the TGA curves for Fe_3O_4 and Fe_3O_4@MAA under N_2 atmosphere. Having considered TGA of Fe_3O_4 and Fe_3O_4@MAA, about 2.34% weight loss differences between 60 to 600 °C is calculated. This weight loss difference is due to the formation of a thin MAA shell around the magnetite core.

A strong bending peak of C—H from $-CH_3$ groups around 1435 cm^{-1} in the Fe_3O_4@AMPH FTIR spectra (Fig. 3A (c)) identified the polymerization in the presence of AIBN as the initiator. A weak peak around 1735 cm^{-1} can be assigned to C═O stretching vibration of carboxyl group which may be due to participation of free MAA in polymerization while two neighboring particles are connected (Fig. 2G). In this case, an MAA bridge between the two particles is formed, its size is increased, and carboxylic groups are added on the surface of the particles. Therefore, Fe_3O_4@AMPH has both hydrophobic (through CH_3 interaction) and hydrophilic (attached carboxylic group) properties. Therefore, amphiphilic MNPs are produced. This is further confirmed by dispersion studies in solvents with different polarities. A 6.11% weight loss of Fe_3O_4@AMPH compare to Fe_3O_4 (Fig. 3B (a), (c)), indicates a thin layer of polymer is coated on the surface and high percent of Fe_3O_4 is remained in the core.

The last product was Fe_3O_4@PMAA. Stretching vibration of carboxyl group around 1738 cm^{-1} in its FTIR spectra (Fig. 3A (d)) clearly shows effective polymerization of MAA and good encapsulation of MNPs in polymeric shells. Fe—O bending vibration peak at 590 cm^{-1} decreases from “a” to “d” in Fig. 3A. This decrease indicates effective hydrogen bonding among organic shells and the inorganic core [20]. C═O vibration peak of carboxylic group at 1738 cm^{-1} that is stronger than the corresponding band in FTIR spectrum of Fe_3O_4@AMPH, indicates abundant carboxylic groups on polymer surface. This is a confirmation for postulated mechanism depicted in Fig. 2H. TGA results of Fe_3O_4@PMAA particles (Fig. 3B(a), (d)) shows about 8.51% weight loss compare to Fe_3O_4. This implied high percent of Fe_3O_4 contents and super paramagnetic properties of the particle.

Overall, the possible mechanism of particle formation has been predicted by FTIR data and confirmed by differences in the sizes of products observed in their TEM and PSA results (Table S1, electronic Supplementary file).

Room temperature magnetic hysteresis loops of the synthesized nanoparticles were also measured to explain their potential application as magnetic sorbents in separation, purification, and pre-concentration methods. Fig. 3C illustrates that all samples are super paramagnetic with a saturation magnetization (SM) of 50.6, 48.5, 36.1 and 25.1 emu g^{-1} for Fe_3O_4, Fe_3O_4@MAA, Fe_3O_4@AMPH, and Fe_3O_4@PMAA, respectively. Among three core-shell samples, Fe_3O_4@MAA has the highest SM value due to the thinnest shell layer. This phenomenon shows that thickness of the shell plays an important role in the SM value of the final MNPs as well as the percent of Fe_3O_4 core in as-prepared particles. Despite the larger size, Fe_3O_4@PMAA has a smaller SM value (lower Fe_3O_4 content). Fe_3O_4@AMPH particles are of intermediate size and have thicker shells, having higher Fe_3O_4 contents (Fig. 3B(c)) in comparison with Fe_3O_4@PMAA and thus have intermediate SM values (Fig. 3C(c)). Fig. 3B(d) identified lower amount of magnetite core in Fe_3O_4@PMAA compared to other modified Fe_3O_4 (Fig. 3B(b and c)) confirming less magnetization in Fe_3O_4@PMAA. However, good magnetic properties allow them to be easily manipulated by an external magnetic field, which is important from an application viewpoint. It was reported that magnetism of materials is highly size dependent [36], in addition to shell thickness. Therefore, the large difference between SM of the polymeric particles, Fe_3O_4@AMPH and Fe_3O_4@PMAA, and the other synthesized particles can be attributed to difference in their size. SM data also confirms that particle size of Fe_3O_4@PMAA is larger than Fe_3O_4@AMPH.

To further evaluate the surface functional groups of Fe_3O_4@AMPH and Fe_3O_4@PMAA and identify their applications, they were dispersed in different solvents. The particles were dispersed by sonication for 5 min. Fig. 4 exhibits photographs of the resultant suspensions captured

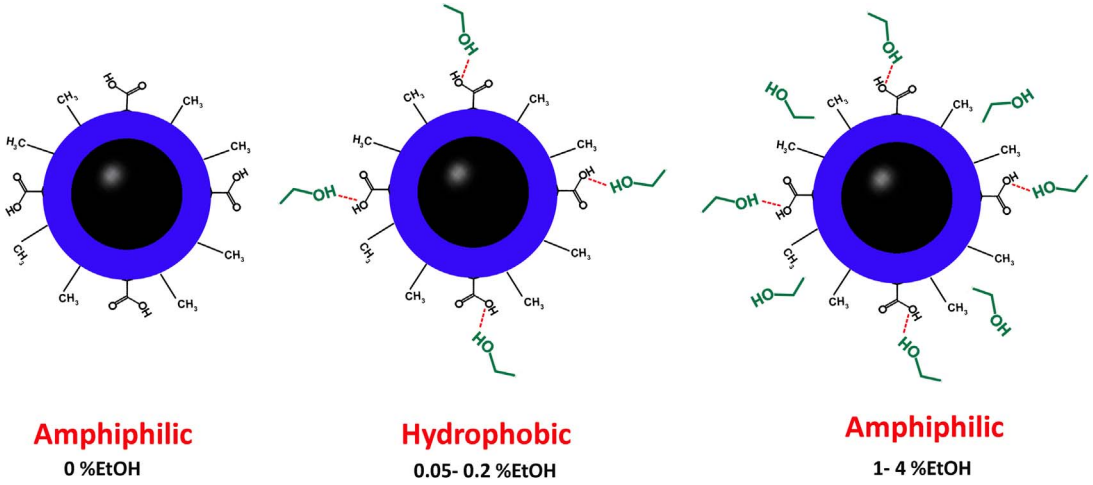

Fig. 5. Behavior of Fe_3O_4@AMPH in 0% (left), 0.05–0.2% (middle) and 1–4% (right) EtOH.

at various time intervals after dispersion of each MNP. In all cases, 10 mL of 1 mg ml^{-1} MNPs was placed in 12 ml glass tubes. Unlike Fe_3O_4@PMAA (Fig. 4 (A)), Fe_3O_4@AMPH has a good dispersion in both water and chloroform after standing for 4 h. This may be attributed to the presence of both nonpolar and polar groups, CH_3 and carboxylic groups, on the surface of Fe_3O_4@AMPH. However, Fe_3O_4@AMPH MNPs can be applied in extraction and separation of analytes in both polar and nonpolar media. In addition, both MNPs were precipitated in propanol, a middle polar solvent, with a polarity index of 3.9 after 4 h (Fig. 4A). With regard to the mechanism reported for sodium oleate bilayer-coated Fe_3O_4 nanoparticles [37] two kind of interaction is assumed for aliphatic alcohols. Their hydrocarbon tails interact with hydrophobic groups such as CH_3 on the surface of the present polymers (hydrophobic interaction) and increase the polarity of the particles. Another interaction is hydrogen bonding with carboxylic group on the surface of the particles. For PrOH hydrogen bonding makes the particle nonpolar and precipitate after 4h (Fig. 4A) while because of low speed of hydrogen bonding hydrophobic interaction predominant and the particles are dispersed in 1h (Fig. 4C). [35]. To further explain dispersivity of Fe_3O_4@AMPH in alcohols with different hydrocarbon chains, dispersion in absolute MeOH, EtOH, and BuOH were also investigated (Fig. 4C). In BuOH and PrOH, with longer hydrocarbon chain, hydrophobic interaction occurs faster than hydrogen bonding. Therefore, speed of precipitation of Fe_3O_4@AMPH in these alcohols is lower than MeOH and EtOH. As Fig. 4C indicates, aggregation of the particles in MeOH and EtOH is faster compared to PrOH and BuOH in 1h. Methanol and ethanol had the same behavior toward the particle. Fast aggregation of such a small alcohol, MeOH and EtOH, is due to their faster tendency for hydrogen bonding with the particles. These alcohols have also the hydrocarbon tails and hydrophobic interaction is possible. So the alcohol content seems effective in the particles dispersion. This hypothesis was proved by dispersing the particles in different V/V% EtOH (Fig. 4D). As it is observed in the figure, the magnetic suspension is stable in EtOH with concentration above 2%. According to the observation and, a mechanism schematically shown in Fig. 5 is suggested. At 0.05–0.2% EtOH, hydrogen bonding of EtOH with carboxylic groups on the particle surface makes the particle non polar, and cause aggregation. As the concentration of EtOH increases, in addition to hydrogen bonding, hydrocarbon tail of the alcohol interact with CH_3 groups on the particle. As a result, particles have lipophilic and hydrophilic groups (have amphiphilic nature) on the surface and is again dispersed in the solution with high EtOH volume percent (Fig. 5). Fig. 4B demonstrates dispersibility of the two polymer in edible oil. The Fe_3O_4@PMAA particles precipitates while Fe_3O_4@AMPH suspension is stable after 1 h. Aggregation of Fe_3O_4@PMAA is due to polar groups on the surfaces.

3.2. Applications

Experiments were conducted to show the possible applications of the resultant MNPs. In a vast variety of applications in core–shell MNPs, the surface of MNPs was modified to increase stability and prevent MNPs aggregation. It made them suitable for being used as a core in polymerization reactions and as sorbents in extraction, purification, and clean-up purposes.

3.2.1. Application of Fe_3O_4@MAA as a support to prepare polymer shell

Abundant double bond on the surface of Fe_3O_4@MAA, makes it ideal core for polymerization reactions. It was shown that Fe_3O_4@MAA is suitable for preparing magnetic molecular imprinted polymers (MMIPs) without using silicon compounds [33]. In MMIPS synthesis, silanization is usually done to aid MNPs surface functionalization [38,39] and is performed in two steps prior to polymerization [40]. In the first step, the silicon compounds with suitable functional groups such as −COO− or −SH are attached to MNPs through interaction with the surface hydroxyl groups of MNPs. In the second step, other silicon compounds are attached to the previously modified MNPs to provide a C=C group at the surface. This reagent is attached to the surface of MNPs by hydrogen band interaction and the resultant MNPs contain abundant reactive surface double bonds and are ready to be used in the MMIPs preparation. Accordingly, Fe_3O_4@MAA MNPs, which contain abundant reactive surface double bonds, are suitable as magnetic cores to support polymer shells. In a previous study conducted by this research group, Fe_3O_4@MAA was used as a magnetic core in preparation of MMIPs for pre-concentration and determination of perphenazine in human urine and plasma samples [33].

3.2.2. Application of Fe_3O_4@PMAA as Ni^{2+} sorbent

Sorbents with suitable functional groups such as −COO−, $-NH_2$, −SH on the surface can interact with certain metal ions and be potentially used in the removal and/or pre-concentration of these ions. Some have been explained in the various literature [41–43]. FTIR and dispersivity studies have shown that Fe_3O_4@PMAA MNPs have carboxyl groups on the surface. These MNPs were tested for their ability to bond with Ni^{2+}. FTIR spectrum of dried Fe_3O_4@PMAA indicates a peak at 1383 cm^{-1} that confirms its ability in nickel uptake (Fig. 3A (e)).

In order to identify the adsorption mechanism for Fe_3O_4@PMAA, Langmuir and Freundlich adsorption isotherms were applied. Linear form of Langmuir adsorption isotherm that was used to calculate the corresponding isotherm equation is:

$$\frac{C_e}{q_e} = \frac{1}{q_m k_L} + \frac{C_e}{q_m}$$

where Ce = the equilibrium concentration of adsorbate (mg/L), q_e = the amount of metal adsorbed per gram of the adsorbent at equilibrium (mg g^{-1}), q_m = maximum monolayer coverage capacity (mg g^{-1}), and K_L = Langmuir isotherm constant (L mg^{-1}). The essential features of the Langmuir isotherm can be expressed in terms of RL, which is a dimensionless constant referred to as separation factor. The $R_L > 1$, $R_L = 1$, $0 < R_L < 1$, and $R_L = 0$ identify unfavorable, linear, favorable, and irreversible adsorption, respectively. Linear form of the empirical equation proposed by Freundlich is

$$\log q_e = \log K_f + \frac{1}{n_f}\log C_e$$

where K_f = Freundlich isotherm constant (L mg^{-1}), n_f = adsorption intensity, Ce = the equilibrium concentration of adsorbate (mg L^{-1}), q_e = the amount of metal adsorbed per gram of the adsorbent at equilibrium (mg g^{-1}). The constant K_f is an approximate indicator of adsorption capacity, while $1/n_f$ determines the adsorption strength in the adsorption process. According to the results listed in Table1, Langmuir isotherm with R^2 equal to 0.9996 is the best description of the adsorption process. The obtained R_L value was between 0 and 1 that indicates favorable adsorption.

First- and second-pseudo-orders models were applied to identify the kinetic of Ni^{2+} adsorption at pH 8. In this pH is higher than pK_a of methacrylic acid, the particles are negatively charged and adsorption of Ni^{2+} becomes feasible [44]. Data were fitted to the first-order and second-order kinetic equations. Data in Table 2 indicate that the second-order model shows the best fit for the experimental data.

In our research group, Fe_3O_4@PMAA has been used for pre-concentration and extraction of Ni^{2+} in real water samples and good results have been obtained.

Table 1
Obtained parameters for Langmuir and Freundlich adsorption isotherms applied to Ni^{2+} uptake by Fe_3O_4@PMAA.

Langmuir				Freundlich		
q_m (mg g^{-1})	K_L (L mg^{-1})	R^2	R_L	$1/n_f$	K_f (L mg^{-1})	R^2
95.24	525	0.9996	0.016	0.1482	145.48	0.8530

Table 2
Kinetic parameters for adsorption of Ni^{2+} on Fe_3O_4@PMAA.

First order kinetic			Second order Kinetic		
K_1	q_e(mg g^{-1})	R^2	K_2	q_e (mg g^{-1})	R^2
0.0034	290.034	0.7395	0.0053	322.5806	0.9997

K_1 and $K_2$are pseudo first and second order rate constant, respectively.

3.2.3. Application of Fe_3O_4@AMPH as sorbent in oily media

Head space sampling is usually a better choice for liquid and solid samples if applicable. While static head space are being used, the volume of the liquid in head space vials should be increased to have a good estimate of VOCs. For cases in which VOCs concentration is low, a pre-concentration technique such as SPME is of vital important. SPME sorbents play an important role in pre-concentration especially when dispersive methods are used. Fe_3O_4@AMPH MNPs are amphiphilic particles and are well dispersed in oily media. However, the ability of Fe_3O_4@AMPH MNPs for separation and pre-concentration of hydrophilic and hydrophobic volatile compounds in heated edible oils was tested. Fig. 6 is GC–MS chromatogram of static head space of different volumes of heated edible oils (Fig. 6A and B) and solid Fe_3O_4@AMPH after contact with heated edible oil as described in Section 2.5. As it can be seen from the total ion chromatogram reported by GC/MS, at least 10 mL of heated edible oil is required to detect the volatile compounds in the oil. The high amount of oil samples may spill around while heating and shaking the vial, adhere to the syringe, then has contaminated the injection port. Fig. 6C illustrates that VOCs desorbed from 5 mg Fe_3O_4@AMPH is approximately the same as those from 10 mL oil head space. Table 3 also lists the VOCs compounds identified by the library of the GC/MS system. The sorption ability of

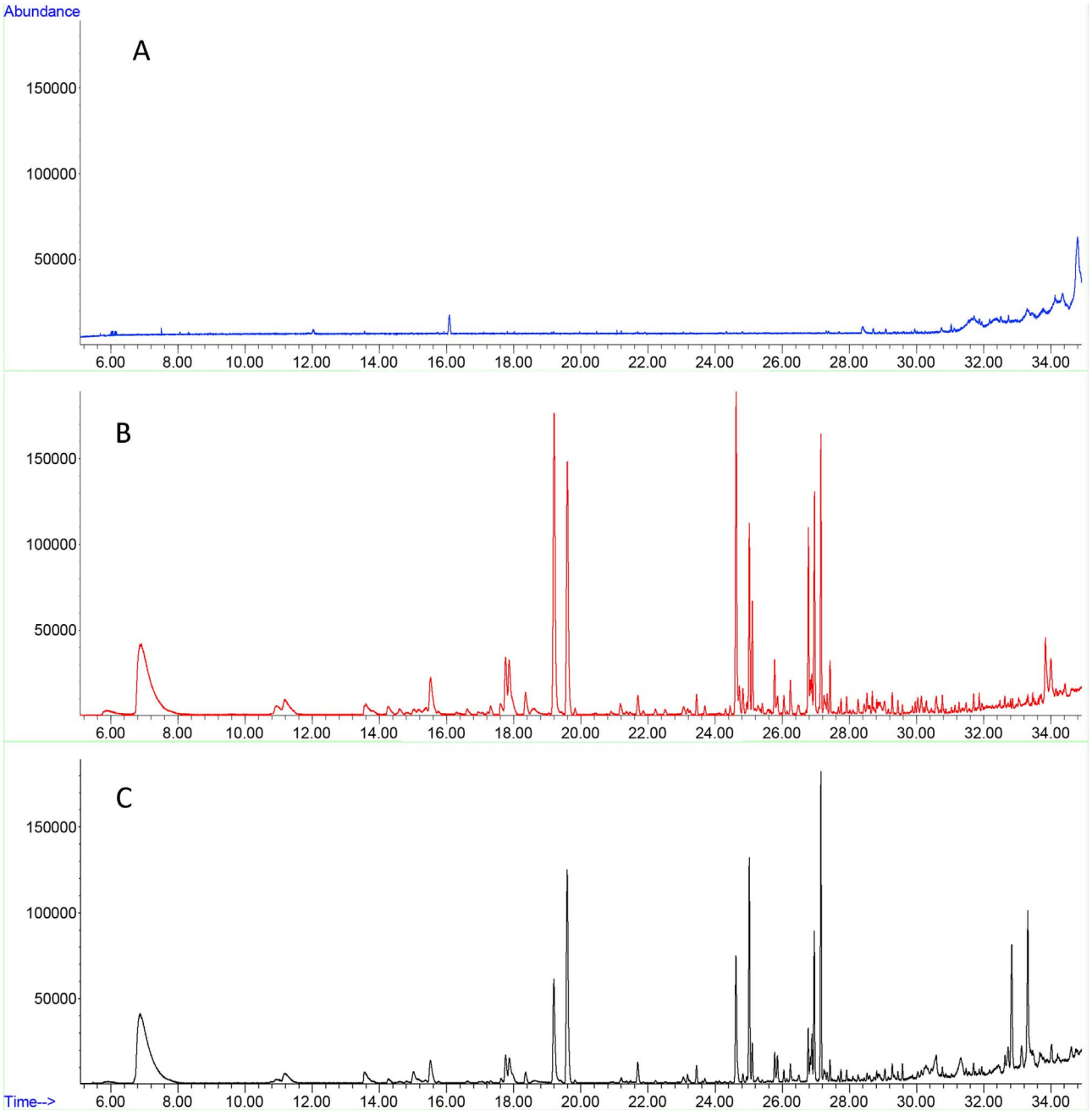

Fig. 6. GC–MS total ion chromatograms of volatile compounds desorbed from head space of A) 0.5 mL and B) 10 mL of heated edible oil, and C) Fe_3O_4@AMPH after adsorption of heated edible oil components.

Table 3
Volatile compounds of heated edible oil determined by static head space GC–MS analysis of different volumes of the oil and Fe_3O_4@AMPH after contact with the oil for ten minutes.

No.	RT	Compound name	% of total area		
			A	B	C
1	6.864	Hexanal	–	19.62	16.47
2	11.193	Heptanal	–	1.31	0.89
3	13.566	2-Heptenal	–	0.8	0.49
4	15.015	3-bromo-Cyclohexene	–	0.62	0.228
5	15.521	4-Methyl-1-pentene	–	1.62	2.20
6	17.760	3-methyl-1-Heptene	–	1.37	2.42
7	18.353	2-methyl-1-pentanol	–	0.56	0.99
8	19.195	2-iodo-3-methyl-Butane	–	5.69	11.79
9	19.591	Cycloheptane	–	10.60	9.46
10	21.698	(E)-2-Nonenal	–	0.87	0.62
11	23.447	(E)-2-Nonen-1-ol	–	0.58	0.51
12	24.620	3,3-dimethyl Hexane	–	4.70	7.97
13	25.017	2-methyl-2-Undecanethiol	–	6.40	4.06
14	25.106	Cyclohexanone	–	1.13	2.43
15	26.77	3,4-dihydro-2H-Pyran	–	1.40	3.57
16	26.881	1-ethyl-1-methyl-Cyclopentane	–	1.24	0.84
17	26.952	3,3,4,4-tetramethyl-2-Pentanone	–	4.05	4.65
18	27.42	3-Methylbutyl 3-methylbutanoate	–	0.47	0.94
19	27.916	2-Nonen-1-ol	–	0.25	0.28
20	29.276	2-methoxy-2-methyl-pentane	–	0.34	0.38

A: 0.5 mL and B: 10 mL heated edible oil; C: 5 mg Fe_3O_4@AMPH after contact with 10 mL heated edible oil.

Fe_3O_4@AMPH can be tuned by the optimization of the separation and pre-concentration conditions. However, this sorbent can effectively adsorb aldehydes and other volatile constituents. Pre-concentration and separation of aldehydes from heated oil by the present sorbent is easier and faster than our previously reported methods [45].

4. Conclusion

To sum up, fast, simultaneous synthesis and modification of Fe_3O_4 in one pot by changes order of addition are introduced. Using Fe_3O_4@MMA in synthesis of molecularly imprinted polymers is economic and reduce the number of steps via elimination of silicon modification of Fe_3O_4. This is the first time that one pot synthesis of Fe_3O_4@PMMA using MAA monomer instead of PMMA is reported. In addition to metal uptake, Fe_3O_4@PMMA has biological and clinical applications. As prepared Fe_3O_4@AMPH has amphoteric properties and is well dispersed in both water and oil. Thus, Fe_3O_4@AMPH can extract hydrophilic and hydrophobic compounds from both aqueous and oily samples.

Acknowledgements

We would like to thank the research deputy of Ahvaz Jundishapur University of Medical Sciences who supported this work under grant number N112 and Iran national Science foundation (INSF) under grant number 95849362. This paper is extracted from Mehdi Safdarian's PhD dissertation.

Appendix A. Supplementary data

Supplementary material related to this article can be found, in the online version, at doi:https://doi.org/10.1016/j.colsurfa.2018.01.004.

References

[1] A. Hajdu, M. Szekeres, I.Y. Toth, R.A. Bauer, J. Mihaly, I. Zupko, E. Tombacz, Enhanced stability of polyacrylate-coated magnetite nanoparticles in biorelevant media, Colloids Surf. B Biointerfaces 94 (2012) 242–249.
[2] Z. Chen, Y. Zhang, S. Zhang, J. Xia, J. Liu, K. Xu, N. Gu, Preparation and characterization of water-soluble monodisperse magnetic iron oxide nanoparticles via surface double-exchange with DMSA, Colloids Surf. A Physicochem. Eng. Aspects 316 (2008) 210–216.
[3] N. Yamauchi, K. Kurumada, Surface hydrophobization of magnetite nanoparticles with polyhexylsilsesquioxane in diethylamine as reaction solvent, Colloids Surfaces A Physicochem. Eng. Aspects 508 (2016) 178–183.
[4] J. Sun, S. Zhou, P. Hou, Y. Yang, J. Weng, X. Li, M. Li, Synthesis and characterization of biocompatible Fe3O4 nanoparticles, J. Biomed. Mater. Res. Part A 80 (2007) 333–341.
[5] P. Azcona, R. Zysler, V. Lassalle, Simple and novel strategies to achieve shape and size control of magnetite nanoparticles intended for biomedical applications, Colloids Surf. A Physicochem. Eng. Aspects 504 (2016) 320–330.
[6] M. Liong, J. Lu, M. Kovochich, T. Xia, S.G. Ruehm, A.E. Nel, F. Tamanoi, J.I. Zink, Multifunctional inorganic nanoparticles for imaging, targeting, and drug delivery, ACS Nano 2 (2008) 889–896.
[7] S. Laurent, D. Forge, M. Port, A. Roch, C. Robic, L. Vander Elst, R.N. Muller, Magnetic iron oxide nanoparticles: synthesis, stabilization, vectorization, physicochemical characterizations, and biological applications, Chem. Rev. 108 (2008) 2064–2110.
[8] C. Huang, B. Hu, Silica-coated magnetic nanoparticles modified with γ-mercaptopropyltrimethoxysilane for fast and selective solid phase extraction of trace amounts of Cd, Cu, Hg, and Pb in environmental and biological samples prior to their determination by inductively coupled plasma mass spectrometry, Spectrochim. Acta Part B At. Spectrosc. 63 (2008) 437–444.
[9] M.H. Mashhadizadeh, Z. Karami, Solid phase extraction of trace amounts of Ag, Cd, Cu, and Zn in environmental samples using magnetic nanoparticles coated by 3-(trimethoxysilyl)-1-propantiol and modified with 2-amino-5-mercapto-1, 3, 4-thiadiazole and their determination by ICP-OES, J. Hazard. Mater. 190 (2011) 1023–1029.
[10] E. Illés, M. Szekeres, E. Kupcsik, I.Y. Tóth, K. Farkas, A. Jedlovszky-Hajdú, E. Tombácz, PEGylation of surfacted magnetite core–shell nanoparticles for biomedical application, Colloids Surf. A Physicochem. Eng. Aspects 460 (2014) 429–440.
[11] N.T. Phan, C.W. Jones, Highly accessible catalytic sites on recyclable organosilane-functionalized magnetic nanoparticles: an alternative to functionalized porous silica catalysts, J. Mol. Catal. A Chem. 253 (2006) 123–131.
[12] S. Zhang, X. Zhao, H. Niu, Y. Shi, Y. Cai, G. Jiang, Superparamagnetic Fe3O4 nanoparticles as catalysts for the catalytic oxidation of phenolic and aniline compounds, J. Hazard. Mater. 167 (2009) 560–566.
[13] T. Madrakian, A. Afkhami, H. Mahmood-Kashani, M. Ahmadi, Superparamagnetic surface molecularly imprinted nanoparticles for sensitive solid-phase extraction of tramadol from urine samples, Talanta 105 (2013) 255–261.
[14] A. Mehdinia, T.B. Kayyal, A. Jabbari, M.O. Aziz-Zanjani, E. Ziaei, Magnetic molecularly imprinted nanoparticles based on grafting polymerization for selective detection of 4-nitrophenol in aqueous samples, J. Chromatogr. A 1283 (2013) 82–88.
[15] S. Yu, G. Wu, X. Gu, J. Wang, Y. Wang, H. Gao, J. Ma, Magnetic and pH-sensitive nanoparticles for antitumor drug delivery, Colloids Surfaces B Biointerfaces 103 (2013) 15–22.
[16] M. Arruebo, R. Fernández-Pacheco, M.R. Ibarra, J. Santamaría, Magnetic nanoparticles for drug delivery, Nano Today 2 (2007) 22–32.
[17] Q. Gao, D. Luo, J. Ding, Y.-Q. Feng, Rapid magnetic solid-phase extraction based on magnetite/silica/poly (methacrylic acid–co–ethylene glycol dimethacrylate) composite microspheres for the determination of sulfonamide in milk samples, J. Chromatogr. A 1217 (2010) 5602–5609.
[18] S.-H. Huo, X.-P. Yan, Facile magnetization of metal–organic framework MIL-101 for magnetic solid-phase extraction of polycyclic aromatic hydrocarbons in environmental water samples, Analyst 137 (2012) 3445–3451.
[19] Y. Liu, H. Li, J.-M. Lin, Magnetic solid-phase extraction based on octadecyl functionalization of monodisperse magnetic ferrite microspheres for the determination of polycyclic aromatic hydrocarbons in aqueous samples coupled with gas chromatography–mass spectrometry, Talanta 77 (2009) 1037–1042.
[20] L. Zhu, C. Li, J. Wang, H. Zhang, J. Zhang, Y. Shen, C. Li, C. Wang, A. Xie, A simple method to synthesize modified Fe3O4 for the removal of organic pollutants on water surface, Appl. Surf. Sci. 258 (2012) 6326–6330.
[21] X. Liu, L. Zhu, X. Gao, Y. Wang, H. Lu, Y. Tang, J. Li, Magnetic molecularly imprinted polymers for spectrophotometric quantification of curcumin in food, Food Chem. 202 (2016) 309–315.
[22] I.S. Ibarra, J.A. Rodriguez, C.A. Galán-Vidal, A. Cepeda, J.M. Miranda, Magnetic solid phase extraction applied to food analysis, J. Chem. 2015 (2015) 1–13.
[23] Y.-Y. Xu, M. Zhou, H.-J. Geng, J.-J. Hao, Q.-Q. Ou, S.-D. Qi, H.-L. Chen, X.-G. Chen, A simplified method for synthesis of Fe3O4@PAA nanoparticles and its application for the removal of basic dyes, Appl. Surf. Sci. 258 (2012) 3897–3902.
[24] S. Kango, S. Kalia, A. Celli, J. Njuguna, Y. Habibi, R. Kumar, Surface modification of inorganic nanoparticles for development of organic–inorganic nanocomposites—A review, Prog. Polym. Sci. 38 (2013) 1232–1261.
[25] J.K. Oh, J.M. Park, Iron oxide-based superparamagnetic polymeric nanomaterials: design, preparation, and biomedical application, Prog. Polym. Sci. 36 (2011) 168–189.
[26] H. Gupta, P. Paul, N. Kumar, S. Baxi, D.P. Das, One pot synthesis of water-dispersible dehydroascorbic acid coated Fe3O4 nanoparticles under atmospheric air: blood cell compatibility and enhanced magnetic resonance imaging, J. Colloid Interface Sci. 430 (2014) 221–228.
[27] Y. Wang, H. Xu, Y. Ma, F. Guo, F. Wang, D. Shi, Facile one-pot synthesis and morphological control of asymmetric superparamagnetic composite nanoparticles, Langmuir ACS J. Surf. Colloids 27 (2011) 7207–7212.
[28] X. Shen, Q. Wang, W. Chen, Y. Pang, One-step synthesis of water-dispersible

cysteine functionalized magnetic Fe3O4 nanoparticles for mercury(II) removal from aqueous solutions, Appl. Surf. Sci. 317 (2014) 1028–1034.
[29] X. Lu, M. Niu, R. Qiao, M. Gao, Superdispersible PVP-coated Fe3O4 nanocrystals prepared by a "One-Pot" Reaction†, J. Phys. Chem. B 112 (2008) 14390–14394.
[30] H. Ai, Layer-by-layer capsules for magnetic resonance imaging and drug delivery, Adv. Drug Deliv. Rev. 63 (2011) 772–788.
[31] E. Baldikova, J. Prochazkova, M. Stepanek, J. Hajduova, K. Pospiskova, M. Safarikova, I. Safarik, PMAA-stabilized ferrofluid/chitosan/yeast composite for bioapplications, J. Magn. Magn. Mater. 427 (2017) 29–33.
[32] B. Küçük, N. Özkan, M. Volkan, Influence of ultrasonically assisted synthesis on particle size of magnetic nanoparticles, J. Phys. Chem. Solids 74 (2013) 1426–1432.
[33] M. Safdarian, Z. Ramezani, A.A. Ghadiri, Facile synthesis of magnetic molecularly imprinted polymer: perphenazine template and its application in urine and plasma analysis, J. Chromatogr. A (2016).
[34] M. Mikhaylova, D.K. Kim, N. Bobrysheva, M. Osmolowsky, V. Semenov, T. Tsakalakos, M. Muhammed, Superparamagnetism of magnetite nanoparticles: dependence on surface modification, Langmuir ACS J. Surf. Colloids 20 (2004) 2472–2477.
[35] A. Ditsch, P.E. Laibinis, D.I. Wang, T.A. Hatton, Controlled clustering and enhanced stability of polymer-coated magnetic nanoparticles, Langmuir ACS J. Surf. Colloids 21 (2005) 6006–6018.
[36] S.-N. Sun, C. Wei, Z.-Z. Zhu, Y.-L. Hou, S.S. Venkatraman, Z.-C. Xu, Magnetic iron oxide nanoparticles: synthesis and surface coating techniques for biomedical applications, Chin. Phys. B 23 (2014) 037503.
[37] M.J. Chen, H. Shen, X. Li, H.F. Liu, Facile synthesis of oil-soluble Fe3O4 nanoparticles based on a phase transfer mechanism, Appl. Surf. Sci. 307 (2014) 306–310.
[38] G. Wang, Y. Fang, P. Kim, A. Hayek, M.R. Weatherspoon, J.W. Perry, K.H. Sandhage, S.R. Marder, S.C. Jones, Layer-by-layer dendritic growth of hyperbranched thin films for surface Sol–Gel syntheses of conformal, functional, nanocrystalline oxide coatings on complex 3D (Bio) silica templates, Adv. Funct. Mater. 19 (2009) 2768–2776.
[39] I.J. Bruce, T. Sen, Surface modification of magnetic nanoparticles with alkoxysilanes and their application in magnetic bioseparations, Langmuir ACS J. Surf. Colloids 21 (2005) 7029–7035.
[40] D. Djozan, B. Ebrahimi, M. Mahkam, M.A. Farajzadeh, Evaluation of a new method for chemical coating of aluminum wire with molecularly imprinted polymer layer. application for the fabrication of triazines selective solid-phase microextraction fiber, Anal. Chim. Acta 674 (2010) 40–48.
[41] H. Bagheri, A. Afkhami, M. Saber-Tehrani, H. Khoshsafar, Preparation and characterization of magnetic nanocomposite of Schiff base/silica/magnetite as a preconcentration phase for the trace determination of heavy metal ions in water, food and biological samples using atomic absorption spectrometry, Talanta 97 (2012) 87–95.
[42] G. Giakisikli, A.N. Anthemidis, Magnetic materials as sorbents for metal/metalloid preconcentration and/or separation, A Rev. Anal. Chim. Acta 789 (2013) 1–16.
[43] F.M. de Oliveira, B.F. Somera, E.S. Ribeiro, M.G. Segatelli, M.J. Santos Yabe, E. Galunin, C.R.T. Tarley, Kinetic and isotherm studies of Ni2+ adsorption on poly (methacrylic acid) synthesized through a hierarchical double-imprinting method using a Ni2+ ion and cationic surfactant as templates, Ind. Eng. Chem. Res. 52 (2013) 8550–8557.
[44] M. Shekarriz, Z. Ramezani, F. Elhami, Preparation and characterization of ZSM5-supported nano-zero-valent iron and its potential application in nitrate remediation from aqueous solution, Int. J. Environ. Sci. Technol. 14 (2017) 1081–1090.
[45] Z. Ramezani, R. Mirzajani, F. Kardani, A novel ultrasound-assisted back extraction reverse micelles method coupled with gas chromatography–flame ionization detection for determination of aldehydes in heated edibles oils, Food Chem. 188 (2015) 30–36.